Macromolecules

pubs.acs.org/Macromolecules Article

Poly(ethylene glycol) Hydrogel Crosslinking Chemistries Identified via Atmospheric Solids Analysis Probe Mass Spectrometry

Kevin J. Endres, Rodger A. Dilla, Matthew L. Becker, and Chrys Wesdemiotis*

Cite This: https://doi.org/10.1021/acs.macromol.1c00765 Read Online

ACCESS | Metrics & More | Article Recommendations | Supporting Information

ABSTRACT: Hydrogels are hydrophilic, crosslinked polymer networks that can absorb several times their own mass in water; they are frequently used in biomedical applications as a native tissue mimic. The characterization of hydrogels and other covalently crosslinked networks is often limited by their insolubility and infinite molecular weight conferred by crosslinking. In this study, chemically crosslinked hydrogel materials based on poly(ethylene glycol) (PEG) have been characterized directly, without any sample preparation, by mild thermal degradation using atmospheric solids analysis probe mass spectrometry (ASAP-MS) coupled with ion mobility (IM) separation and tandem mass spectrometry (MS/MS) characterization of the degradants. The structural insight gained from these experiments is illustrated with the analysis of oxime-crosslinked PEG hydrogels formed by the click reaction between 4-arm PEG star polymers with either ketone or aminooxy end group functionalities and PEG dimethacrylate (PEGDMA) copolymeric hydrogel networks formed by photopolymerization of PEGDMA. The ASAP-MS, IM, and MS/MS methods were combined to identify the crosslinking chemistry and obtain precursor chemistry information retained in the end-group substituents of the thermal degradation products.

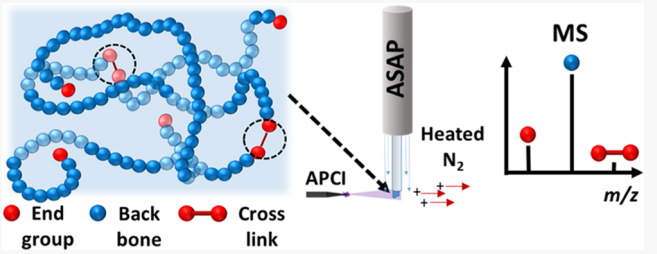

INTRODUCTION

Polymer networks are materials formed by the crosslinking of polymer chains and have applications ranging from rubber tires to tissue engineering scaffolds.[1,2] As with all polymeric materials, the final properties are influenced by microstructural factors, such as the reactant polymer molecular weight, chain dispersity, chemical composition, and crosslinker identity.[3,4] These factors contribute specific features to the network; for example, networks with shorter chains (i.e., higher crosslinking density) yield stiffer, less flexible materials than networks with longer chains (i.e., lower crosslinking density).[5] Once the network is formed, the material is no longer soluble as the molecular weight trends toward infinity.[6]

Crosslinking can be achieved by either physical or chemical means, each providing a variety of unique structure−property relationships. Physically crosslinked polymers are reinforced through secondary bonding interactions such as hydrogen bonding,[2,6−8] ionic bonding,[9−12] and crosslinking crystallization.[13,14] In contrast, chemical crosslinking involves the formation of covalent bonds between polymer precursors and/or linker molecules. Synthetic pathways to covalently bound materials include (but are not limited to) crosslinking by radical polymerization in the presence of photoinitiators,[15,16] radical propagation after hydrogen abstraction by high-energy irradiation,[16,17] condensation reactions,[18,19] addition reactions,[18,19] and click chemistry reactions.[20−25] The extent of crosslinking varies depending on the types of reactive groups and their respective locations within the polymers. For example, crosslinking can occur in the backbone, side chains, and the end groups of polymer chains, making bonding combinations potentially complex depending on the location and number of reactive sites.

A specific subcategory of crosslinked materials that can be synthesized using the aforementioned chemistries is hydrogels, named for their ability to absorb and retain water within their hydrophilic polymer matrix.[26−28] These materials are typically only 1−30 wt % polymers, yet they can absorb up to ∼80 times their initial mass of water in some cases.[29] Applications of hydrogels include contact lenses,[28] wound dressings, hygiene products,[30] tissue engineering scaffolds,[26,30] and drug delivery vehicles.[30] For biomedical applications, poly(ethylene glycol) (PEG) is ubiquitous in hydrogel materials because of its limited immunogenicity and ease of functionalization with various reactive groups.[26,27] The mechanical properties of PEG hydrogels can easily be changed, either by varying the weight percent of the material or by creating defects within the network. Furthermore, the attachment of small, bioactive

Received: April 8, 2021
Revised: July 15, 2021

Scheme 1. (a) Oxime Hydrogels from Click Chemistry between 10 kDa 4-Arm PEG Star Precursors and (b) Polymethacrylate (PMA)−PEG Hydrogels from Radical Polymerization of 4 kDa PEGDMA[a]

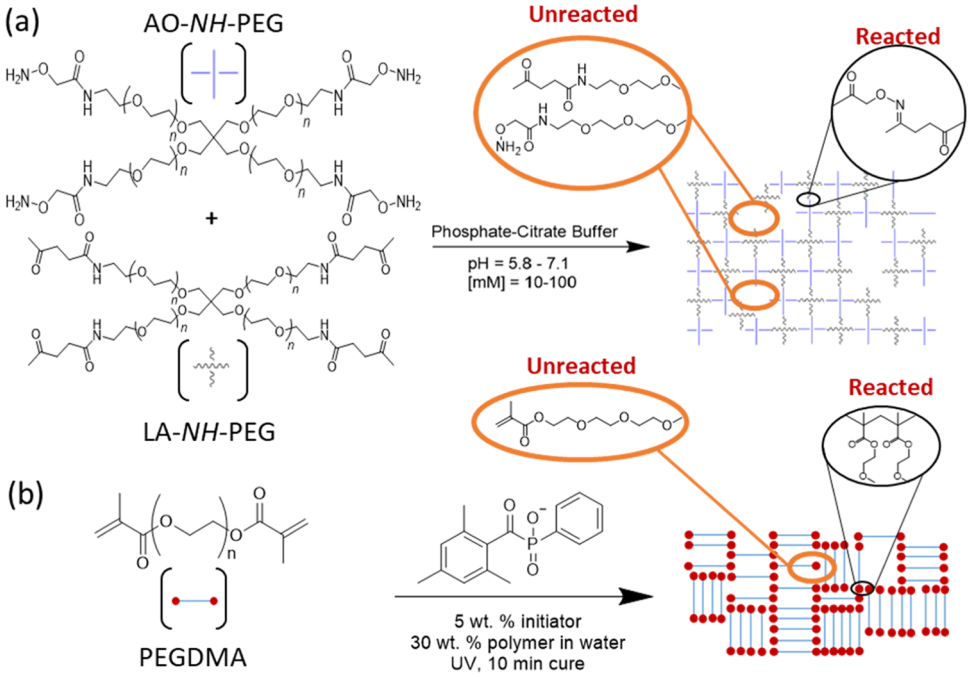

[a]In the star PEG precursors shown in (a), the end groups are attached through amide bonds. Precursors with the end groups attached via ester bonds were also studied.

peptide sequences has made PEG hydrogels an ideal material for investigating cell−material interactions.[29,31]

Hydrogel formation is typically verified by inverted tube tests or small angle oscillatory shear rheology (SAOS); the latter technique probes the transition of material properties at the gelation point, which change from a primarily viscous to a primarily elastic response.[32] SAOS, tensile testing, and compression tests are also used to determine the mechanical properties, which are often compared to swelling and small-angle neutron scattering data to investigate the gel microstructure.[29,31] None of these techniques, however, provides information about specific chemical crosslinking within the material. Furthermore, while hydrogel crosslinking is easily performed, the insolubility of the resultant network typically prevents utilizing most routine chemical characterization techniques (e.g., UV-vis, NMR, and so forth) without some form of degradation. Johnson and co-workers, for example, developed an asymmetrically degrading hydrogel system, wherein the crosslinking junctions could be resolved by liquid chromatography coupled with mass spectrometry (LC−MS), providing chemical and morphological information simultaneously.[33]

Generally, extremely high molecular weights prevent straightforward MS analysis. Information about the composition of chemically crosslinked materials and their additive and stabilizer contents has traditionally been gained via thermal desorption/degradation and MS analysis of the desorbates and degradants with or without prior gas chromatography (GC) separation.[34−42] Often, this approach lacks the ability to identify the nature of the crosslinking chemistry and precursor functionality. This problem may be bypassed by employing lower temperatures, as performed in direct probe atmospheric pressure chemical ionization (DP-APCI) MS; when applied to chemically or physically crosslinked polyurethane (PU)−polydimethylsiloxane (PDMS) copolymers, this method yielded low-molecular-weight oligomeric fragments that detailed the composition of the copolymers, indicating at least one pathway to successful MS analysis of crosslinked materials.[43]

Another pyrolysis/ionization variant is the atmospheric solids analysis probe (ASAP). This source contains a heated capillary in which solids or liquids can be deposited for thermal desorption/degradation; the capillary is heated by a stream of nitrogen gas and is located within an APCI source for in situ ionization of desorption and degradation products.[44] Compared to conventional pyrolysis probes, the ASAP source is operated at relatively low temperatures (≤500 °C), yielding not only monomeric but also oligomeric species that provide molecular connectivity detail. Further microstructural verification and complementary information on the thermal stability and degradation pathways of the polymer can be gained by tandem mass spectrometry (MS/MS) experiments.[39−41] In the past 13 years, ASAP-MS and ASAP-MS/MS have been used extensively to characterize polymer additives as well as diverse, relatively low molecular weight synthetic polymers,[44−48] including PEG,[45] polystyrene,[45] PU,[47] and PDMS.[48] An ASAP source combined with ion mobility (IM)-MS adds potential to separate desorbate and degradant ions by their size and shape,[49−51] thus enhancing the analytical information obtainable from mild thermal degradation experiments.[52−57] The added IM dimension enables the separation of isobaric and isomeric species and also permits determination of their collision cross-section (CCS) values, which provide a quantitative insight about their 3D size/shape. The ASAP-IM-MS hyphenation has been used to characterize and/or differentiate the degree of unsaturation, microstructure, and architecture of ASAP pyrolyzates from polyethylene (PE), PE/polyester blends, polypropylene, and poly(α-olefin)s.[52,54−57]

https://doi.org/10.1021/acs.macromol.1c00765
Macromolecules XXXX, XXX, XXX−XXX

Combining ASAP-MS with MS/MS and IM creates an effective top-down technique for the analysis of polymeric materials that are difficult to characterize at the molecular level by other analytical techniques. These methods were utilized in this study to address persisting structural questions about the crosslinking microstructures in networks formed from PEG. The thermal degradation mechanisms and pyrolyzate products of PEG have been elucidated by GC−MS, FTIR spectroscopy, and matrix-assisted laser desorption/ionization (MALDI) MS.[39,58] According to these studies, this polymer decomposes via free radical chemistry initiated by homolytic C−O and C−C bond scissions (cf. Scheme S1). Homolytic cleavage of a C−O bond produces C- and O-centered radicals; the former produce either ethyl ether- or vinyl ether-terminated products through hydrogen abstraction or hydrogen loss, respectively, whereas the latter form hydroxyl (−OH)- or aldehyde-terminated products via the same reactions. On the other hand, homolytic C−C bond cleavage produces two methylene radicals that ultimately yield methyl ether end groups through hydrogen abstraction.[39,58] This knowledge is essential for interpreting the spectra acquired in our study to determine the molecular connectivity and confirm the primary structure of two types of hydrogels (Scheme 1), viz. (a) oxime-crosslinked PEG hydrogels formed by the click reaction between 4-arm PEG stars with levulinamide (LA-*NH*) or levulinic acid (LA-*O*) end groups and 4-arm PEG stars with aminoxyacetamide (AO-*NH*) or aminooxyacetic acid (AO-*O*) end groups (the crosslinking end-group functionalities in these gels were attached to the PEG stars by amide or ester bonding);[59,60] and (b) crosslinked PEG dimethacrylate (PEGDMA) copolymer hydrogels formed by radical propagation in the presence of a lithium acylphosphazine (LAP) photoinitiator and UV light.[61] ASAP-MS enabled direct characterization of these two covalently crosslinked PEG hydrogels, unveiling crosslinking chemistry and precursor chemistry information retained in pyrolyzate end groups. IM-MS allowed for the separation of different polymer constituents overlapping at the same mass, while MS/MS provided the pyrolyzate microstructure and end-group verification.

EXPERIMENTAL SECTION

Materials. Alcohol- or aminooxy-terminated 4-arm 10 kDa PEG variants were purchased from Creative PEGWorks (Chapel Hill, NC). 4 kDa PEGDMA was purchased from Monomer-Polymer and Dajac Labs (Trevose, PA). All other reagents and solvents were purchased from Sigma-Aldrich (St. Louis, MO) or Fisher Scientific (Waltham, MA) and used as received unless noted otherwise. All reactions were performed under nitrogen unless noted otherwise.

Synthesis of 4-Arm Ketone-Functionalized 10 kDa PEG. LA-*NH*-PEG was prepared as previously described.[59] Briefly, 10 kDa 4-arm PEG (5.02 g, 0.5 mmol, 1 equiv) was functionalized with LA-*NH* (0.291 g, 2.51 mmol, 5 equiv) via diisopropylcarbodiimide (DIC)-mediated esterification using DIC (0.316 g, 2.50 mmol, 5 equiv) and 4-(dimethylamino)pyridinium 4-toluene sulfonate (DPTS) (0.074 g, 0.250 mmol, 0.5 equiv) as catalysts and dichloromethane (75 mL) as the solvent. All reagents except DIC were dissolved in a round-bottom flask under a nitrogen atmosphere, and the reaction mixture was cooled to 0 °C on an ice bath for 15 min before the dropwise addition of DIC. The reaction proceeded for 12 h before gravity filtration and purification by precipitation into methanol (3×), followed by precipitation into ether, with centrifugation steps in-between each precipitation. The product was dried under vacuum overnight. LA-*O*-PEG was prepared similarly by replacing LA-*NH* with LA-*O* .

Synthesis of 4-Arm Aminooxy-Functionalized 10 kDa PEG. AO-*NH*-PEG was prepared as previously described.[60] Briefly, 10 kDa 4-arm PEG (5.02 g, 0.5 mmol, 1 equiv) was functionalized with (*tert*-butyloxycarbonyl (Boc)-aminooxy)acetamide (0.291 g, 2.51 mmol, 5 equiv) via DIC-mediated esterification using DIC (0.316 g, 2.50 mmol, 5 equiv) and DPTS (0.074 g, 0.250 mmol, 0.5 equiv) as catalysts and dichloromethane (75 mL) as the solvent. All reagents except DIC were dissolved in a round-bottom flask under a nitrogen atmosphere, and the reaction mixture was cooled to 0 °C on an ice bath for 15 min before the dropwise addition of DIC. The reaction proceeded for 12 h before gravity filtration and purification by precipitation into methanol (3×), followed by precipitation into ether, with centrifugation steps in-between each precipitation. The Boc-protected intermediate was then dried under vacuum overnight. To yield the final aminooxy product, the Boc-protected product was dissolved in 10 mL of 4 M HCl/dioxane under nitrogen flow and stirred overnight. The final product was recovered by precipitation into diethyl ether and dried under vacuum. AO-*O*-PEG was prepared similarly by using (Boc-aminooxy)acetic acid instead of (Boc-aminooxy)acetamide.

MS Experiments. A quadrupole/time-of-flight mass spectrometer equipped with a traveling-wave IM accessory and an ASAP source (Synapt G1, Waters Corp., Manchester, UK) was used to perform all analyses. This instrument contains three successive stacked ring ion guides between the Q and ToF analyzers, called the trap cell (closest to Q), IM cell, and transfer cell (closest to ToF). All MS/MS experiments were performed in the transfer cell post-IM separation. The instrument has been described in detail elsewhere.[62]

Open-ended glass capillaries (Bibby Scientific Ltd, Stone, Staffordshire, UK) were utilized in the ASAP experiments to accommodate sample positioning adjacent to the mass spectrometer inlet (cf. Scheme S2). Prior to sample introduction, the capillaries were wiped with Kimtech Kimwipes and baked in the ion source at 500 °C for 2 min to avoid any residual contamination originating from the capillary manufacture and storage. A crosslinked material of roughly the same size as the inner diameter of the glass capillary (1.3 mm) was then inserted into the end of the capillary and positioned in-line with the APCI source and the mass spectrometer inlet (Scheme S2).

The ASAP source was operated in a positive mode using the V resolution mode over the m/z range 50−2500. The corona discharge was set to 15 μA, the sampling cone to 35 V, the extraction cone to 3.2 V, the nitrogen gas flow to 900 L/h, and the source temperature to 120 °C. The temperature of the nitrogen gas which provides the heat needed for thermal desorption and degradation was increased stepwise at 50 °C/min from 100 to 500 °C for gradient heating. Isothermal heating was performed at 450 °C. Both modes resulted in very similar spectra; therefore, only the data from isothermal heating are presented and discussed. A 20 mL scintillation vial filled with HPLC-grade methanol was placed inside the source to promote protonation. IM experiments were performed using a nitrogen gas flow of 22.7 mL/min through the IM cell; the traveling wave height and the traveling wave velocity were 35 V and 350 m/s, respectively. The argon gas flow through the trap and transfer collision cells was 1.5 mL/min. The trap and transfer cell collision energies were set to 6 and 4 eV, respectively, in the MS mode. For MS/MS analysis, the transfer cell collision energy was increased to 20 eV to induce collisionally activated dissociation.

Before each experiment, the mass spectrometer was externally calibrated with sodium iodide solution (0.2 mg/mL) using an electrospray ionization source. Common $[H−PEG−OH + H]^+$ peaks were utilized as internal standards for accurate mass determinations. Data acquisition and mass spectral interpretation were performed using the Waters MassLynx (version 4.1) and DriftScope (version 2.8) programs.

Hydrogel Fabrication. Oxime hydrogels (O-*X*-PEG; -*X*-: -*NH*- or -*O*-) (1 mL volume) were prepared by separately dissolving either LA-*NH*-PEG (69.1 mg, 0.007 mmol) and AO-*NH*-PEG (68.1 mg, 0.007 mmol) or LA-*O*-PEG (77.4 mg, 0.007 mmol) and AO-*O*-PEG (76.2 mg, 0.007 mmol) in 500 μL of citric acid/phosphate buffer at pH 5.7, 6.8, or 7.1 (all precursors had a M_w of ∼10 kDa). The PEG solutions were then mixed and allowed to sit at room temperature

https://doi.org/10.1021/acs.macromol.1c00765
Macromolecules XXXX, XXX, XXX−XXX

until gelation occurred (1−22 h). PMA−PEG gels were prepared from 15 wt % PEG-dimethacrylate (M_n of ∼4.0 kDa) in deionized H_2O using 2.5 wt % LAP photoinitiator, which was prepared as previously described.[63] The solution was then placed in a UV oven (EnvisionTEC, Dearborn, MI; 70 W, 55 Hz, and λ_{max} = 400 nm) for 5 min to cure.

RESULTS AND DISCUSSION

Oxime-Crosslinked PEG Hydrogels. The products observed in the ASAP-MS spectra of these networks with a virtually infinite molecular weight correspond to shorter PEG oligomers (<1000 Da) formed by thermal degradation of the interconnected PEG chains (cf. Scheme S1). The substituents identified in these oligomers by mass measurement and MS/MS (vide infra) conclusively reveal whether the pyrolyzates originate from the reacted or unreacted segments of the hydrogel. The reacted segment contains the oxime functionality, whereas unreacted segments contain the ketone or aminooxy functionalities of the hydrogel precursors (Scheme 1). To facilitate the characterization of the PEG pyrolyzates, a vial of methanol was placed inside the ASAP source to promote ionization by protonation (cf. Scheme S2). The CH_3OH vapor forms protonated methanol clusters, $(CH_3OH)_nH^+$, which readily transfer a proton to polyethers. Since the gels were swollen with water, protonated water clusters were also present in the ASAP source to serve as protonation agents of the PEG pyrolyzates. Charge exchange with $N_2^{\bullet+}$ ions to produce radical ions of the pyrolyzates also occurs in the ASAP source; its extent depends on the molecular structure of the pyrolyzate, which controls its ionization energy versus proton affinity.

Figures 1 and S1 depict the ASAP-MS spectra of the crosslinked hydrogel and its two precursors (i.e., the ketone- and aminooxy-functionalized star polymers). Figure S1 shows the entire spectra, which include singly charged oligomeric ions in the m/z 400−1000 range along with low mass internal ions typical of the PEG connectivity (protonated cyclic n-mers with n = 2−5); Figure 1 depicts an expanded view of these spectra covering the m/z 545−600 window and displaying the various $[PEG + H]^+$ (or $PEG^{\bullet+}$) distributions detected within one repeat unit.

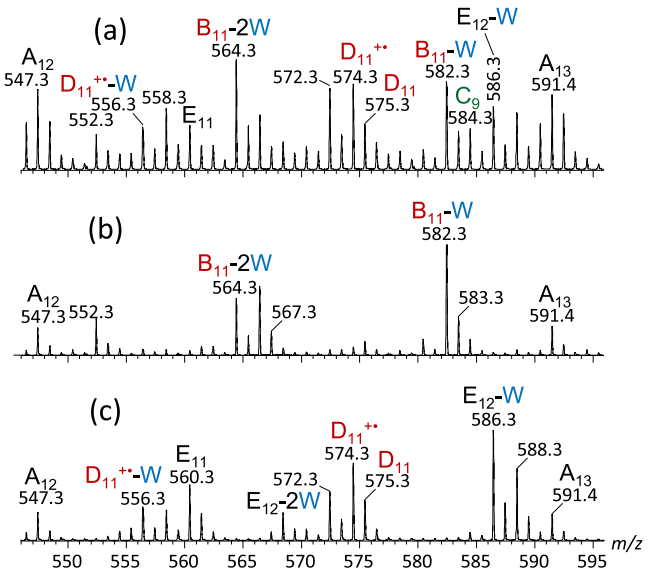

Figure 1. Zoomed-in ASAP-MS spectra (m/z 545−600) of the (a) chemically crosslinked oxime hydrogel, (b) 4-arm PEG star precursor with LA-*NH* end groups, and (c) 4-arm PEG star precursor with AO-*NH* end groups. See Figure S1 for the entire spectra and Table 1 for the proposed structures of distributions A_n−E_n.

Five different PEG distributions are observed from the crosslinked hydrogel (labeled A_n−E_n in Figure 1a). Some of them are also present in the ASAP-MS spectra of the 4-arm precursors used to synthesize the hydrogel (Figure 1b,c) and hence must arise from unreacted segments of the hydrogel that still contain the original end groups. Accurate mass measurement of the ions in Figure 1a−c indicate the molecular compositions and proposed structures summarized in Table 1 (see Table S1 for a list of the measured and calculated m/z data).

The PEG pyrolyzates contain −OH or $-OCH{=}CH_2$ end groups (cf. Table 1). Such terminal substituents arise from the homolytic cleavage of the $-CH_2CH_2O-CH_2CH_2-$ ether bonds in the PEG backbone to $-CH_2CH_2O^{\bullet}$ + $^{\bullet}CH_2CH_2-$ radicals that subsequently undergo $H^{\bullet}$ abstraction and $H^{\bullet}$ loss, respectively, or $H^{\bullet}$ transfer between the detached fragments, to yield −OH- and vinyl-terminated chains. Additionally, vinyl-terminated oligomers can be generated by water (W) loss from the −OH termini. For this reason and for brevity, the $-OCH{=}CH_2$ ending chains in Figure 1 are designated as B_n−W, D_n−W, or E_n−W, irrespective of their formation mechanism. It is reminded at this point that the *NH* label in the abbreviated structures (Table 1) indicates keto (LA), aminooxy (AO), or oxime (O) functionality attachment to PEG via amide bonds.

Figure 1 displays a direct comparison of the spectra obtained from the 4-arm star-branched precursors and the reacted gel, allowing for differentiation of the signature ions formed from each structure. The C_n ion at m/z 584.3 in the mass spectrum of the crosslinked material (Figure 1a) matches the composition $[O\text{-}NH\text{-}PEG_9 + H]^+$ (i.e., $[O\text{-}NH\text{-}(CH_2CH_2O)_9-H + H]^+$), in which the oxime connectivity is retained as a substituent to PEG_9 (Table 1); note that the oxime group may be a central substituent to the overall nine repeat units (as shown in Table 1), or an end group to a contiguous PEG_9 block, depending on what bonds were broken during thermal degradation (vide infra). Similarly, the B_n−W ion at m/z 582.3 (Figure 1a,b) agrees well with protonated $LA\text{-}NH\text{-}PEG_{11}-H_2O$ (i.e., $[LA\text{-}NH\text{-}(CH_2CH_2O)_{10}-CH{=}CH_2 + H]^+$), whereas the $D_n^{\bullet+}$ radical ion at m/z 574.3 (Figure 1a,c) matches $[AO\text{-}NH\text{-}PEG_{11}]^{\bullet+}$ (i.e., $[AO\text{-}NH\text{-}(CH_2CH_2O)_{11}-H]^{\bullet+}$). These assignments are validated by the ASAP-MS spectrum of the gel prepared using ester bonds to connect the keto, aminooxy, and oxime functionalities to PEG (Figure S2), where the ions at m/z 584.3 (C_9), 582.3 (B_{11}−W), and 574.3 ($D_{11}^{\bullet+}$) shift to m/z 586.4, 583.4, and 575.4, respectively, due to *NH* (15 Da) → *O* (16 Da) replacement (Table S2).

Series C_n reveals that crosslinks remain intact during mild thermal degradation and confirms the oxime chemistry of the crosslinked gel. Series B_n and $D_n^{\bullet+}$ verify the presence of defects ("loose ends" or unreacted ends) in the network. Series A_n and E_n can arise from crosslinked as well as defective regions; the former only contains a PEG segment, while the latter contains PEG attached to a piece of the aminooxy functionality resulting from N−O bond cleavage within the aminooxy precursor and/or crosslinked material. It is noteworthy that the ketone (i.e., LA-*NH*)-substituted PEG chains also undergo a second water loss (cf. Figure 1a,b, as well as

https://doi.org/10.1021/acs.macromol.1c00765
Macromolecules XXXX, XXX, XXX−XXX

Table 1. Proposed Pyrolyzate Structures Observed by ASAP-MS of Oxime-Crosslinked Hydrogels (Amide Connectivity in Reactants)

Series [a]	Proposed Structure [b]	Chemical origin
A_n	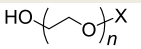	Network backbone (PEG)
B_n	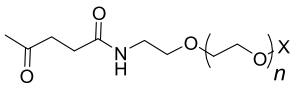	Levulinamide end group (LA-*NH*-PEG)
C_n	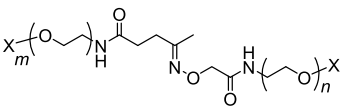	Oxime crosslink (O-*NH*-PEG)
D_n	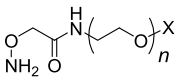	Aminooxy end group (AO-*NH*-PEG)
E_n	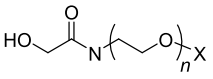	Fragmented precursor end group or crosslink

[a]PEG series in Figure 1 observed in the form of $[M + H]^+$or $M^{\bullet+}$ ions. For a list of measured and calculated m/z values, see Table S1. [b]X = H or $-CH{=}CH_2$.

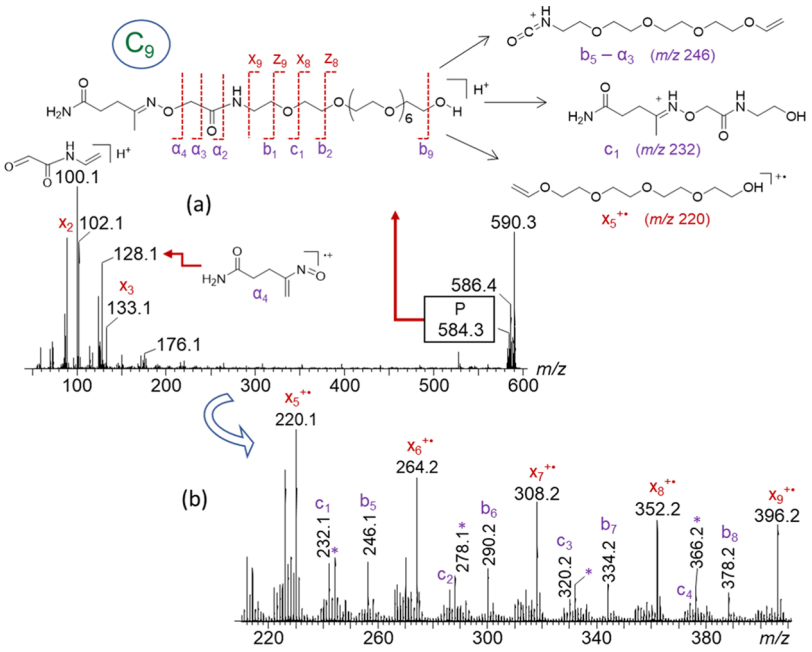

Figure 2. (a) ASAP-MS/MS spectrum of the pyrolyzate $[O\text{-}NH\text{-}PEG_9{-}H + H]^+$ (C_9 ion at m/z 584.3) and (b) zoomed view of the m/z 210–410 window. The C_9 ion structure with an associated fragment nomenclature is shown on top of the full MS/MS spectrum. Peak assignments correspond to the cleavages labeled in the structure.[66] Cleavages of the PEG bonds give rise to b_n and c_n fragments (they retain the oxime substituent) or x_n and z_n fragments (they contain the free −OH end group). Bond cleavages within the oxime substituent give rise to α_n fragments or losses of α_n pieces. The insets in (a) show the structures proposed for the internal fragment at m/z 100.1 and the unique fragment at m/z 128.1 which includes a large part of the oxime functionality. The dominant fragment series in (b) are c_n with the entire oxime substituent and −OH as end groups (see c_1 in the top scheme), $b_n{-}\alpha_3$ (labeled as b_n for brevity) with part of the oxime substituent and vinyl end groups, and $x_n^{\bullet+}$ with vinyl and −OH end groups. The series marked by * are $c_n{-}\alpha_2$ ions, and the unlabeled series correspond to various types of internal fragments.

S1a,b); this reaction is attributed to the LA-*NH* group, as levulinamide itself shows abundant water loss (but insignificant ammonia loss) in its electron ionization mass spectrum.[64]

Additional evidence for the formation of oxime groups in the crosslinked gel was sought by MS/MS analysis of the 9-mer from distribution C_n (m/z 584.3 in Figure 1a). Although C_n and the other pyrolysis products listed in Table 1 stand out in the ASAP-MS spectra (Figure 1), it is worth noting that many more minor pyrolyzates are formed, convoluting the spectra, especially for the crosslinked material which shows small peaks at essentially every m/z value (cf. Figure 1a vs 1b or 1c). Due to this complexity, the main pyrolysis products may contain

https://doi.org/10.1021/acs.macromol.1c00765
Macromolecules XXXX, XXX, XXX−XXX

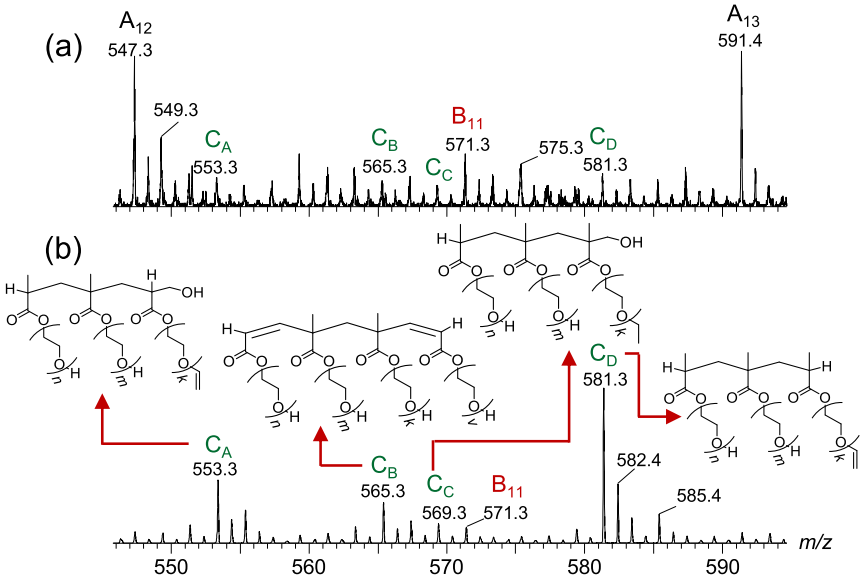

Figure 3. Zoomed-in ASAP-MS spectra (m/z 545−600) of (a) photochemically crosslinked PMA−PEG hydrogel and (b) degraded PMA−PEG hydrogel. A_n corresponds to $[HO-(CH_2CH_2O)_n-H + H]^+$ ions; B_{11} corresponds to $[MA-(CH_2CH_2O)_{11}-H + H]^+$ ions originating from the PEGDMA precursor [MA = $CH_2C(CH_3)CO(=O)O$]; and C_{A-D} correspond to crosslinked $[PMA_x-PEG_y + H]^+$ ions with the proposed comb-like structures indicated above each labeled peak and $x = n + m + k$ $(+v) = 6$ or 7.

small admixtures of such "background" components which usually are PEG degradation products. The low concentration of the latter degradants does not significantly affect the mass measurement of the main pyrolyzates, for which individual, resolved peaks were selected for the determination of their m/z. For MS/MS, on the other hand, a broad m/z window (~5 Da) was subjected to fragmentation to increase the sensitivity and obtain a useable spectrum. Adventitious PEG pyrolyzates were admitted into the collision cell during this process, giving rise to superimposed minor fragment series. For this reason, only the major fragment series in the ASAP-MS/MS spectrum of C_9 will be discussed here, which fortunately provided sufficient structural information to verify the structure derived from mass measurements.

The MS/MS spectrum of C_9 (Figure 2) shows four dominant fragment series: c_n, $b_n-\alpha_3$ (labeled as b_n on the spectrum for brevity), $c_n-\alpha_2$ (labeled by *), and $x_n^{\bullet+}$. Series c_n contains the entire oxime functionality on truncated PEG chains with a free −OH end group (see scheme on top of Figure 2), whereas series $b_n-\alpha_3$ and $c_n-\alpha_2$ contain part of the oxime group on truncated PEG chains with either a vinyl ($b_n-\alpha_3$) or −OH ($c_n-\alpha_2$) end group, respectively; α_2 and α_3 indicate which bonds within the oxime group were cleaved to create the fragment. Finally, series $x_n^{\bullet+}$ consists of short PEG chains with vinyl and −OH end groups and no oxime component; they are probably coproduced with the other fragments after the initial C−O bond cleavage in the PEG chain. The c_n fragment series provides strong evidence that the C_n pyrolyzates contain an intact oxime substituent with the structural elements of the precursors used to form crosslinking oxime bonds. The fragment at m/z 128 (α_4 in Figure 2), which contains the elements of an oxime bond, substantiates this conclusion. Overall, the MS/MS data confirm the oxime chemistry of the crosslinked gel. The MS/MS fragments have been rationalized from a C_n structure in which the oxime substituent is an end group (as in Figure 2), but similar fragmentation patterns would arise from a C_n pyrolyzate in which the oxime group is a central substituent (as shown in Table 1). The observation of $b_n-\alpha_3$, $c_n-\alpha_2$, and $x_n^{\bullet+}$ ions with long PEG_n chains (up to $n = 9$ for C_9) points out that a major proportion of C_n contains the oxime functionality as an end group. Such a structure would emerge if C−N bonds are cleaved more readily than C−O bonds upon thermal degradation of the crosslinked gel (cf. C_n structure in Table 1); the lower bond energy of C−N versus C−O bonds (305 vs 358 kJ/mol, respectively) justifies this expectation.[65]

Although the spectra in Figures 1 and 2 confirm the presence of a crosslinked polymer and unveil the type of crosslinking chemistry, their relative intensities cannot be used to quantify the amount of crosslinking. The reasons include incomplete pyrolysis, ionization biases, and in-source material loss. As in all MS-based characterization techniques, quantitative analysis will require calibration of the intensity scale with standards, which will be investigated in a future study.

Photochemically Crosslinked PMA−PEG Hydrogels. As a copolymer, the PMA−PEG hydrogel presents an added level of complexity. Nevertheless, the strategy employed for the oxime hydrogel, viz. a combination of ASAP-MS and MS/MS, permits a confident characterization of crosslink chemistry and defects also for this more complicated copolymeric system. In this case, successful crosslinking creates PMA chains that are absent in the PEGDMA precursor. Hence, any PMA segments detected in the thermal degradation products must result from the crosslinked material, whereas PEG chains with an original methacrylate (MA) end group would indicate unreacted (loose) ends.

ASAP-MS analysis of the PMA−PEG hydrogel (Figure S3) shows the appearance of an abundant PEG distribution with −OH and −H end groups after isothermal heating for >3 min (series A_n in Figure S3d). An expanded view of the m/z 545−600 region (Figure 3a), which was assayed in detail for the oxime gels, reveals the presence of several additional distributions composed of different end groups and/or substituents. The spectrum in Figure 3b was acquired from the same sample after 10 weeks; over this period, the material

https://doi.org/10.1021/acs.macromol.1c00765
Macromolecules XXXX, XXX, XXX−XXX

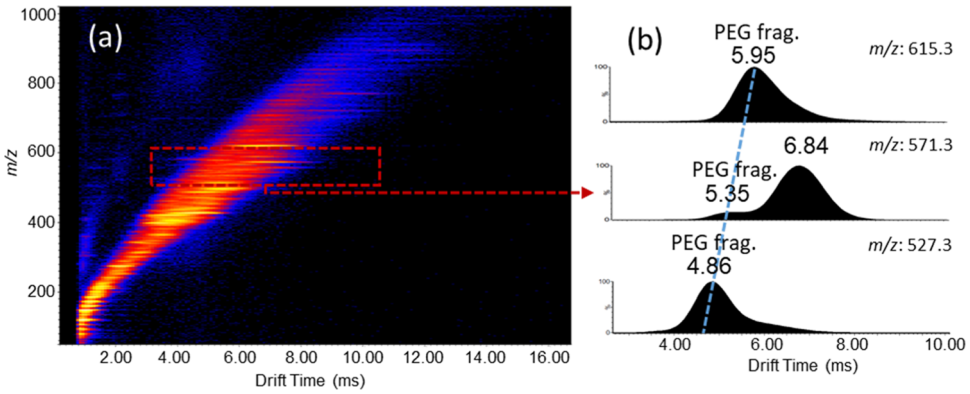

Figure 4. (a) ASAP-IM-MS mobilogram showing drift time separation of pyrolyzates formed from the nondegraded copolymeric PMA−PEG gel and (b) extracted drift time distributions ("chromatograms") of m/z 615.3 (top, B_{12}), 571.3 (center, B_{11} + PMA_4 isobar), and 527.3 (bottom, B_{10}). The blue dashed line denotes the drift time trend of PEG fragments differing by one repeating unit.

had undergone hydrolytic degradation into a mixture of solid gel and viscous liquid components. The ASAP-MS spectrum of the degraded sample (Figure 3b) displays a dramatic improvement in the signal-to-noise ratio due to removal of chemical noise and ionization enhancement of pyrolyzates that potentially contain crosslinking information. The masses of the enhanced peaks (Table S3) revealed compositions indicative of PEG chains from the network backbone (A_{12} and A_{13} in Figure 3a), MA-substituted PEG oligomers from unreacted chain ends (B_{11} in Figure 3), as well as PMA_x−PEG_y copolymeric degradants from crosslinked regions (C_A, C_B, C_C, and C_D), cf. Table S4. Meanwhile, MALDI-MS characterization of the 10 week old mixture confirmed the formation of short PEG chains with −OH and −H end groups during hydrogel degradation, cf. Figure S4.

A de novo approach was taken again to reconcile the pyrolysis pattern of the PMA−PEG network (Figure 3) based on the known thermal degradation behavior of PMA and PEG backbones (Schemes S3 and S1, respectively).[39,41] Homolytic bond cleavages within the PMA and PEG backbones, followed by hydrogen abstraction or loss, lead to shorter chains terminating with saturated or unsaturated substituents. In ASAP experiments of hydrocarbon chains, homolytic bond cleavage may be accompanied by radical oxidation to yield −OH groups.[56,67] Such reactions in the crosslinked PMA−PEG gel would generate degradants with a comb polymer architecture; predicted structures that agree well with the measured m/z values (Table S3) are shown above the corresponding C_{A-D} peaks in Figure 3b. Trimeric or tetrameric PMA chains predominate within the m/z range ionized via ASAP due to their stability; these products appear in distributions with the 44 Da repeating, resulting from homolytic bond cleavages in the PEG ester chains of the gel.

To elucidate the crosslink chemistry of the PMA−PEG hydrogel, MS/MS was utilized to verify the structure of the B_{11} and C_{A-D} pyrolyzates observed in the m/z 545−600 window. The presence of two different polymer chains in the PMA−PEG gel increases the probability of forming isobaric products upon thermal degradation. Although a minor isobaric admixture with a PEG pyrolysis product does not obstruct MS/MS analysis (vide supra), a major byproduct at the same nominal m/z ratio would disable characterization of an overlapping pyrolyzate. The ASAP product mixture was therefore examined by IM-MS, where the ions formed after thermal degradation are separated by both their m/z ratio and their drift time through the IM cell. The resulting ion mobilogram (Figure 4a) displays singly charged PEG ions and reveals significant isobar overlap in select m/z ranges but not across the entire mobilogram phase space. For the pyrolyzates observed in the m/z 545−600 window, isobaric ions are clearly discerned only for m/z 571.3 (labeled B_{11} in Figure 3), as illustrated by its extracted drift time chromatogram in Figure 4b where it is contrasted with the drift time chromatograms of two homologues with one PEG repeat unit added (B_{12} at m/z 615.3) or removed (B_{10} at m/z 527.3). The corresponding drift time trend (blue dashed line in Figure 4b) strongly suggests that the m/z 571.3 ion drifting at 5.35 ms is B_{11}, while the m/z 571.3 ion drifting at 6.84 ms must be a different species with a larger CCS. The ASAP-IM-MS/MS spectra of these two isobaric ions confirm this expectation, cf. Figure 5.

The ASAP-IM-MS/MS spectrum of the faster m/z 571.3 component corroborates the structure $[MA-(CH_2CH_2O)_{11}-H + H]^+$ (B_{11}) assigned by mass measurements (cf. Figure 5a). Very similar IM-MS/MS spectra are obtained for the B_{10} (m/z 527.3) and B_{12} (m/z 615.3) homologues (Figure S5). These ions must originate from unreacted PEGDMA or from unreacted (defect) segments of the gel, as they contain an unpolymerized MA end group. On the other hand, the ASAP-IM-MS/MS spectrum of the more slowly drifting m/z 571.3 ion (Figure 5b) is inconsistent with PEG connectivity, as also suggested by the absence of a 44 Da repeating pattern in the drift time chromatograms of Figure 4b. This m/z 571.3 was observed initially upon continued isothermal heating at 450 °C, but its relative intensity varies as the material is continuously heated (cf. Figure S3).

The abundant MS/MS fragment at m/z 147.1 in Figure 5b cannot originate from PEG because of the absence of fragments either higher or lower in mass by 14 Da (CH_2); it is, however, consistent with a structure carrying a trimethylbenzoyl group, $C_9H_{11}CO-$, which is part of the photoinitiator used for PMA polymerization and crosslinking (cf. Scheme 1b). The photoinitiator generates trimethylbenzoyl radicals that initiate PMA formation by addition to the MA end group of the PEGDMA gel precursor. Hence, this m/z 571.3 component is attributed to a PMA_4 degradant with no complete PEG unit (cf. Figure 5b). Such oligomers have been shown to readily depolymerize to small, stable fragment ions upon collisionally activated MS/MS dissociation.[66] Furthermore, the small fragments by losses of CO_2 and $C_9H_{11}COOH$ validate such a product (cf. Scheme S4). Since a

https://doi.org/10.1021/acs.macromol.1c00765
Macromolecules XXXX, XXX, XXX−XXX

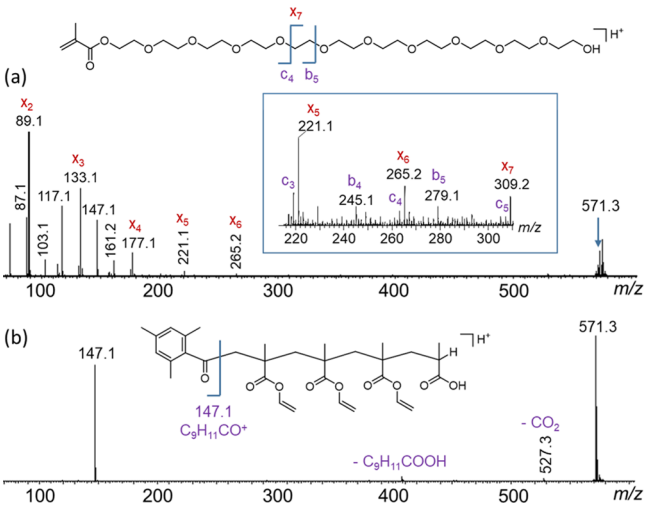

Figure 5. ASAP-IM-MS/MS spectra of m/z 571.3 ions with drift times of (a) 5.35 ms (B_{11}) and (b) 6.84 ms (PMA_4), cf. Figure 4b. Encased in (a) is a zoomed-in view of the m/z 210−320 region. The insets show the molecular structures unveiled by the MS/MS fragmentation patterns; b_n and c_n fragments contain the MA substituent and a $-CH{=}CH_2$ or $-CH_2CH_2OH$ group, respectively, at the other chain end (the latter fragments were termed c_n'' previously,[66] but the double prime is omitted here to avoid crowding); x_n fragments contain the free −OH group and a vinyl group at the other chain end. The not labeled peaks at m/z < 200 in (a) are internal fragments. A block sequence of vinyl MA and methacrylic acid is shown in (b), but any other sequence is equally possible.

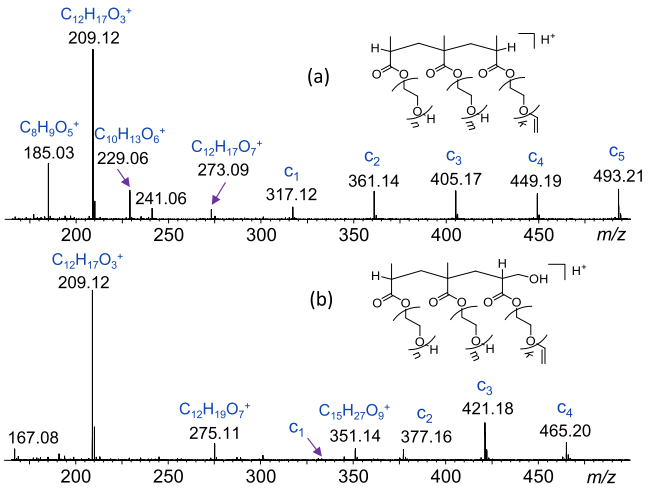

Figure 6. ASAP-MS/MS spectra (m/z 170−500 region) of comb-shaped pyrolyzate ions (a) $[PMA_3{-}PEG_7 + H]^+$ at m/z 581.3 (C_D in Figure 3) and (b) $[PMA_3{-}PEG_6 + H]^+$ at m/z 553.3 (C_A in Figure 3) from thermal degradation of the PMA−PEG hydrogel. The proposed precursor ion structures are included in each MS/MS spectrum ($n + m + k = 7$ in C_D and 6 in C_A). Full spectra are shown in Figure S6. The c_n series arises by O−C bond cleavages in the PEG side chains, which give rise to truncated −OH-terminating chains.[66] See Table S5 for plausible structures of the fragments marked by their chemical formulae.

PMA chain is only present in the crosslinked hydrogel, this species provides strong evidence that photochemical crosslinking of PEGDMA has taken place.

The ASAP-MS/MS spectra of the two most abundant pyrolyzate ions that potentially contain crosslinking information, viz. C_D and C_A in Figure 3b, are shown in Figure 6a,b, respectively. In both cases, contiguous c_n fragment series are observed, which diagnose −OH-terminating PEG chains, as well as fragments characteristic of PMA segments denoted by their chemical formulae on top of the corresponding peaks; possible structures of the latter fragments are included in Table S5. Very similar features are found in the ASAP-MS/MS spectra of pyrolyzates C_B (m/z 565.3) and C_C (m/z 569.3), which are presented in Figure S7. Overall, the MS/MS fragments provide strong evidence for the comb-like PMA−PEG structure proposed for C_A−C_D, authenticating the crosslinking chemistry of this photochemically produced gel.

It is noteworthy that the C_A−C_D pyrolyzates produce a common, abundant fragment at m/z 209, which can serve as a signature ion for the PMA frame, as it is absent from the MS/MS spectra of B_n (PEGDMA precursor), cf. Figures 6, S6, and S7 versus 5a and S5. On the other hand, abundant x_n fragments in the middle and upper mass range of the MS/MS spectra signify unlinked PEG chains with a free −OH group, (cf. Figures 5a and S5), whereas abundant c_n fragments are indicative of PEG pendants in the PMA−PEG comb pyrolyzates (cf. Figures 6, S6, and S7). These results underscore the ability of MS/MS fragmentation to reveal important structural attributes.

CONCLUSIONS

The combination of ASAP, which encompasses mild thermal degradation and soft ionization, with high-resolution mass analysis, MS/MS fragmentation, and IM separation was shown to be a powerful method for the molecular characterization of PEG-based hydrogel materials, including hydrogels formed by a click reaction between 4-arm PEG stars with ketone or aminooxy functionalities at their end groups, or by photochemically induced radical polymerization of PEG with vinyl end groups. This study is the first application of the ASAP methodology to crosslinked polymer networks. These materials were initially broken down and ionized via pyrolysis and APCI to yield oligomeric PEG pyrolyzate ions in the m/z 300−1100 range. MS/MS isolation and fragmentation were subsequently utilized to verify their primary structure and elucidate their crosslink bonding characteristics based on the substituents detected and identified in the pyrolyzates. Signature c_n and b_n fragment ions gave microstructure information about the end groups of the observed PEG chains, helping to delineate their structure and origin. Similarly, MS/MS gave rise to reference ions with PMA connectivity, most prominently m/z 209.1, which provided direct evidence for PMA−PEG comb copolymer pyrolyzates. The IM dimension allowed for signal deconvolution and, combined with MS/MS, for conclusive identification of isobaric pyrolyzates, one containing the photoinitiator attached to a short PMA chain and the other an unreacted methacrylate chain end. The described analytical method is of particular interest for the characterization of crosslinked materials that lack tools suitable for their efficient and effective chemical analysis and can thermally degrade below 500 °C. This method may be useful in deformulation studies of unknown precursor and crosslinking chemistry and is applicable to more complex polymeric networks crosslinked with different chemistries, such as those formed from paint formulations.[68] Finally, the method

https://doi.org/10.1021/acs.macromol.1c00765
Macromolecules XXXX, XXX, XXX−XXX

also reveals insights about the thermal decomposition properties of the crosslinked material under study, which could be important for hydrogels used under extreme conditions, for example, in fireproof materials and for fire extinguishing.[69,70]

The presented methodology establishes a novel analytical route for the qualitative analysis of crosslinked polymeric networks. Relative quantitation is also possible by comparing similar networks prepared under different conditions to determine the extents of crosslinking versus unreacted (unlinked) loops. Absolute quantitation of the latter features would require the addition of a known quantity of a standard to a precisely known amount of the sample analyzed, so that peak intensities can be compared quantitatively. This aspect is currently under investigation and will be reported in a separate study.

■ ASSOCIATED CONTENT

Supporting Information

The Supporting Information is available free of charge at https://pubs.acs.org/doi/10.1021/acs.macromol.1c00765.

Thermal decomposition pathways of PEG and polyacrylates; ASAP scheme; measured m/z data; pyrolyzate oligomers detected; full ASAP-MS spectra; ASAP-MS spectrum of the prepared oxime hydrogel; MS/MS spectrum of the oxime bond containing pyrolyzate; MALDI-MS analysis of the degraded PMA−PEG hydrogel; MS/MS spectra of select pyrolyzates from the PMA−PEG hydrogel; and MS/MS fragmentation scheme for PMA chains (PDF)

■ AUTHOR INFORMATION

Corresponding Author

Chrys Wesdemiotis − *Department of Polymer Science, The University of Akron, Akron, Ohio 44325, United States; Department of Chemistry, The University of Akron, Akron, Ohio 44325, United States;* orcid.org/0000-0002-7916-4782; Email: wesdemiotis@uakron.edu

Authors

Kevin J. Endres − *Department of Polymer Science, The University of Akron, Akron, Ohio 44325, United States;* Present Address: DuPont Specialty Products, Wilmington, DE 19803, Unites States; orcid.org/0000-0002-0857-6966

Rodger A. Dilla − *Department of Chemistry, Duke University, Durham, North Carolina 27708, United States;* Present Address: Bridgestone Americas, Inc, Akron, Ohio 44301, Unites States

Matthew L. Becker − *Department of Chemistry, Duke University, Durham, North Carolina 27708, United States;* orcid.org/0000-0003-4089-6916

Complete contact information is available at: https://pubs.acs.org/10.1021/acs.macromol.1c00765

Notes

The authors declare no competing financial interest.

■ ACKNOWLEDGMENTS

Support from the National Science Foundation (CHE-1808115 to C.W.) is gratefully acknowledged.

■ REFERENCES

(1) Nasir, M.; Teh, G. K. The effects of various types of crosslinks on the physical properties of natural rubber. *Eur. Polym. J.* **1988**, *24*, 733−736.

(2) Sun, J.-Y.; Zhao, X.; Illeperuma, W. R. K.; Chaudhuri, O.; Oh, K. H.; Mooney, D. J.; Vlassak, J. J.; Suo, Z. Highly stretchable and tough hydrogels. *Nature* **2012**, *489*, 133−136.

(3) Seymour, R. B.; Carraher, C. E., Jr. *Structure—Property Relationships in Polymers*; Springer: Boston, MA, 1984.

(4) Shonaike, G. O.; Advani, S. G. *Advanced Polymeric Materials: Structure Property Relationships*, 1; CRC Press: Boca Raton, FL, 2003.

(5) Flory, P. J.; Rehner, J., Jr. Statistical mechanics of crosslinked polymer networks I. Rubberlike elasticity. *J. Chem. Phys.* **1943**, *11*, 512−520.

(6) Stockmayer, W. H. Theory of molecular size distribution and gel formation in branched polymers II. General cross linking. *J. Chem. Phys.* **1944**, *12*, 125−131.

(7) Bell, C. L.; Peppas, N. A. Modulation of drug permeation through interpolymer complexed hydrogels for drug delivery applications. *J. Controlled Release* **1996**, *39*, 201−207.

(8) Mathur, A. M.; Hammonds, K. F.; Klier, J.; Scranton, A. B. Equilibrium swelling of poly(methacrylic acid-g-ethylene glycol) hydrogels. *J. Controlled Release* **1998**, *54*, 177−184.

(9) Polk, A.; Amsden, B.; de Yao, K.; Peng, T.; Goosen, M. F. A. Controlled release of albumin from chitosan-alginate microcapsules. *J. Pharm. Sci.* **1994**, *83*, 178−185.

(10) Liu, L.-S.; Liu, S.-Q.; Ng, S. Y.; Froix, M.; Ohno, T.; Heller, J. Controlled release of interleukin-2 for tumour immunotherapy using alginate/chitosan porous microspheres. *J. Controlled Release* **1997**, *43*, 65−74.

(11) Chenite, A.; Chaput, C.; Wang, D.; Combes, C.; Buschmann, M. D.; Hoemann, C. D.; Leroux, J. C.; Atkinson, B. L.; Binette, F.; Selmani, A. Novel injectable neutral solutions of chitosan form biodegradable gels in situ. *Biomaterials* **2000**, *21*, 2155−2161.

(12) Janes, K. A.; Fresneau, M. P.; Marazuela, A.; Fabra, A.; Alonso, M. J. Chitosan nanoparticles as delivery systems for doxorubicin. *J. Controlled Release* **2001**, *73*, 255−267.

(13) Yokoyama, F.; Masada, I.; Shimamura, K.; Ikawa, T.; Monobe, K. Morphology and structure of highly elastic poly-(vinyl alcohol) hydrogel prepared by repeated freezing-and-melting. *Colloid Polym. Sci.* **1986**, *264*, 595−601.

(14) Stenekes, R. J. H.; Talsma, H.; Hennink, W. E. Formation of dextran hydrogels by crystallization. *Biomaterials* **2001**, *22*, 1891−1898.

(15) Langer, R. S.; Peppas, N. A. Present and future applications of biomaterials in controlled drug delivery systems. *Biomaterials* **1981**, *2*, 201−214.

(16) Decker, C. Photoinitiated crosslinking polymerisation. *Prog. Polym. Sci.* **1996**, *21*, 593−650.

(17) Caliceti, P.; Salmaso, S.; Lante, A.; Yoshida, M.; Katakai, R.; Martellini, F.; Mei, L. H. I.; Carenza, M. Controlled release of biomolecules from temperature-sensitive hydrogels prepared by radiation polymerization. *J. Controlled Release* **2001**, *75*, 173−181.

(18) Hennink, W. E.; van Nostrum, C. F. Novel crosslinking methods to design hydrogels. *Adv. Drug Delivery Rev.* **2012**, *64*, 223−236.

(19) Akhtar, M. F.; Hanif, M.; Ranjha, N. M. Methods of synthesis of hydrogels. A review. *Saudi Pharm. J.* **2016**, *24*, 554−559.

(20) Hoyle, C. E.; Lee, T. Y.; Roper, T. Thiol-Enes: Chemistry of the past with promise for the future. *J. Polym. Sci., Part A: Polym. Chem.* **2004**, *42*, 5301−5338.

(21) Ossipov, D. A.; Hilborn, J. Poly(vinyl alcohol)-based hydrogels formed by "click chemistry". *Macromolecules* **2006**, *39*, 1709−1718.

(22) Malkoch, M.; Vestberg, R.; Gupta, N.; Mespouille, L.; Dubois, P.; Mason, A. F.; Hedrick, J. L.; Liao, Q.; Frank, C. W.; Kingsbury, K.; Hawker, C. J. Synthesis of well-defined hydrogel networks using click chemistry. *Chem. Commun.* **2006**, *0*, 2774−2776.

(23) Crescenzi, V.; Cornelio, L.; Di Meo, C.; Nardecchia, S.; Lamanna, R. Novel Hydrogels via click chemistry: Synthesis and

potential biomedical applications. *Biomacromolecules* **2007**, *8*, 1844−1850.
(24) Nimmo, C. M.; Shoichet, M. S. Regenerative Biomaterials that "Click": Simple, aqueous-based protocols for hydrogel synthesis, surface immobilization, and 3D patterning. *Bioconjugate Chem.* **2011**, *22*, 2199−2209.
(25) Grover, G. N.; Lam, J.; Nguyen, T. H.; Segura, T.; Maynard, H. D. Biocompatible hydrogels by oxime click chemistry. *Biomacromolecules* **2012**, *13*, 3013−3017.
(26) Slaughter, B. V.; Khurshid, S. S.; Fisher, O. Z.; Khademhosseini, A.; Peppas, N. A. Hydrogels in regenerative medicine. *Adv. Mater.* **2009**, *21*, 3307−3329.
(27) Zhu, J. Bioactive modification of poly(ethylene glycol) hydrogels for tissue engineering. *Biomaterials* **2010**, *31*, 4639−4656.
(28) Hoteling, A. J.; Nichols, W. F.; Harmon, P. S.; Conlon, S. M.; Nuñez, I. M.; Hoff, J. W.; Cabarcos, O. M.; Steffen, R. B.; Hook, D. J. Characterization and quantitation of PVP content in a silicone hydrogel contact lens produced by dual-phase polymerization processing. *J. Biomed. Mater. Res., Part B* **2018**, *106*, 1064−1072.
(29) Hu, X.; Vatankhah-Varnoosfaderani, M.; Zhou, J.; Li, Q.; Sheiko, S. S. Weak hydrogen bonding enables hard, strong, tough, and elastic hydrogels. *Adv. Mater.* **2015**, *27*, 6899−6905.
(30) Caló, E.; Khutoryanskiy, V. V. Biomedical applications of hydrogels: A review of patents and commercial products. *Eur. Polym. J.* **2015**, *65*, 252−267.
(31) Lutolf, M. P.; Hubbell, J. A. Synthetic biomaterials as instructive extracellular microenvironments for morphogenesis in tissue engineering. *Nat. Biotechnol.* **2005**, *23*, 47−55.
(32) Song, H. Y.; Faust, L.; Son, J.; Kim, M.; Park, S. J.; Ahn, S.-k.; Wilhelm, M.; Hyun, K. Small and medium amplitude oscillatory shear rheology of model branched polystyrene (PS) melts. *Polymers* **2020**, *12*, 365.
(33) Zhou, H.; Woo, J.; Cok, A. M.; Wang, M.; Olsen, B. D.; Johnson, J. A. Counting primary loops in polymer gels. *Proc. Natl. Acad. Sci. U.S.A.* **2012**, *109*, 19119−19124.
(34) Wampler, T. P.; Levy, E. J. Effects of slow heating rates on products of polyethylene pyrolysis. *Analyst* **1986**, *111*, 1065−1067.
(35) Montaudo, G.; Puglisi, C. Thermal degradation mechanisms in condensation polymers. In *Developments in Polymer Degradation-7*; Grassie, N., Ed.; Elsevier Applied Science: London, 1987; pp 35−80.
(36) Lattimer, R. P. Direct analysis of elastomer compounds by soft ionization, tandem (MS/MS) and high resolution (AC-MS) mass spectrometry. *Rubber Chem. Technol.* **1995**, *68*, 783−793.
(37) Lattimer, R. P.; Polce, M. J.; Wesdemiotis, C. MALDI-MS analysis of pyrolysis products from a segmented polyurethane. *J. Anal. Appl. Pyrolysis* **1998**, *48*, 1−15.
(38) Carroccio, S.; Puglisi, C.; Montaudo, G. Thermal degradation mechanisms of polyetherimide investigated by direct pyrolysis mass spectrometry. *Macromol. Chem. Phys.* **1999**, *200*, 2345−2355.
(39) Lattimer, R. P. Mass spectral analysis of low-temperature pyrolysis products from poly(ethylene glycol). *J. Anal. Appl. Pyrolysis* **2000**, *56*, 61−78.
(40) Lattimer, R. P. Mass spectral analysis of low-temperature pyrolysis products from poly(tetrahydrofuran). *J. Anal. Appl. Pyrolysis* **2001**, *57*, 57−76.
(41) Lattimer, R. P. Pyrolysis mass spectrometry of acrylic acid polymers. *J. Anal. Appl. Pyrolysis* **2003**, *68*−*69*, 3−14.
(42) Trimpin, S.; Wijerathne, K.; McEwen, C. N. Rapid methods of polymer and polymer additives identification: multi-sample solvent-free MALDI, pyrolysis at atmospheric pressure, and atmospheric solids analysis probe mass spectrometry. *Anal. Chim. Acta* **2009**, *654*, 20−25.
(43) Whitson, S. E.; Erdodi, G.; Kennedy, J. P.; Lattimer, R. P.; Wesdemiotis, C. Direct probe-atmospheric pressure chemical ionization mass spectrometry of cross-linked copolymers and copolymer blends. *Anal. Chem.* **2008**, *80*, 7778−7785.
(44) McEwen, C. N.; McKay, R. G.; Larsen, B. S. Analysis of solids, liquids, and biological tissues using solids probe introduction at atmospheric pressure on commercial LC/MS instruments. *Anal. Chem.* **2005**, *77*, 7826−7831.
(45) Smith, M. J. P.; Cameron, N. R.; Mosely, J. A. Evaluating atmospheric pressure solids analysis probe (ASAP) mass spectrometry for the analysis of low molecular weight synthetic polymers. *Analyst* **2012**, *137*, 4524−4530.
(46) Du, Z.; Zhang, Y.; Li, A.; Lv, S. Rapid identification of polymer additives by atmospheric solid analysis probe with quadrupole time-of-flight mass spectrometry. *Rapid Commun. Mass Spectrom.* **2014**, *28*, 2035−2042.
(47) Lebeau, D.; Ferry, M. Direct characterization of polyurethanes and additives by atmospheric solid analysis probe with time-of-flight mass spectrometry (ASAP-TOF-MS). *Anal. Bioanal. Chem.* **2015**, *407*, 7175−7187.
(48) Fouquet, T.; Barrère-Mangote, C.; Farenc, M.; Afonso, C.; Giusti, P. Atmospheric solid analysis probe mass spectrometry vs electrospray tandem mass spectrometry of polydimethylsiloxanes in positive and negative ionization modes. *Rapid Commun. Mass Spectrom.* **2015**, *29*, 982−986.
(49) *Ion Mobility Spectrometry−Mass Spectrometry: Theory and Applications*; Wilkins, C. L., Trimpin, S., Eds.; CRC Press: Boca Raton, FL, 2010.
(50) Lanucara, F.; Holman, S. W.; Gray, C. J.; Eyers, C. E. The power of ion mobility-mass spectrometry for structural characterization and the study of conformational dynamics. *Nat. Chem.* **2014**, *6*, 281−294.
(51) *Advances in Ion Mobility-Mass Spectrometry: Fundamentals, Instrumentation and Applications*; Donald, W. A., Prell, J. S., Eds.; Elsevier B.V.: Amsterdam, Netherlands, 2019.
(52) Barrère, C.; Maire, F.; Afonso, C.; Giusti, P. Atmospheric solid analysis probe-ion mobility mass spectrometry of polypropylene. *Anal. Chem.* **2012**, *84*, 9349−9354.
(53) Barrère, C.; Hubert-Roux, M.; Afonso, C.; Racaud, A. Rapid analysis of lubricants by atmospheric solid analysis probe-ion mobility mass spectrometry. *J. Mass Spectrom.* **2014**, *49*, 709−715.
(54) Barrère, C.; Selmi, W.; Hubert-Roux, M.; Coupin, T.; Assumani, B.; Afonso, C.; Giusti, P. Rapid analysis of polyester and polyethylene blends by ion mobility-mass spectrometry. *Polym. Chem.* **2014**, *5*, 3576−3582.
(55) Cossoul, E.; Hubert-Roux, M.; Sebban, M.; Churlaud, F.; Oulyadi, H.; Afonso, C. Evaluation of atmospheric solid analysis probe ionization coupled to ion mobility mass spectrometry for characterization of poly(ether ether ketone) polymers. *Anal. Chim. Acta* **2015**, *856*, 46−53.
(56) Farenc, M.; Witt, M.; Craven, K.; Barrère-Mangote, C.; Afonso, C.; Giusti, P. Characterization of polyolefin pyrolysis species produced under ambient conditions by Fourier transform ion cyclotron resonance mass spectrometry and ion mobility-mass spectrometry. *J. Am. Soc. Mass Spectrom.* **2017**, *28*, 507−514.
(57) Mendes Siqueira, A. L.; Beaumesnil, M.; Hubert-Roux, M.; Loutelier-Bourhis, C.; Afonso, C.; Bai, Y.; Courtiade, M.; Racaud, A. Atmospheric solid analysis probe coupled to ion mobility spectrometry-mass spectrometry, a fast and simple method for polyalphaolefin characterization. *J. Am. Soc. Mass Spectrom.* **2018**, *29*, 1678−1687.
(58) Voorhees, K. J.; Baugh, S. F.; Stevenson, D. N. An Investigation of the thermal degradation of poly(ethylene glycol). *J. Anal. Appl. Pyrolysis* **1994**, *30*, 47−57.
(59) Zander, Z. K.; Hua, G.; Wiener, C. G.; Vogt, B. D.; Becker, M. L. Control of mesh size and modulus by kinetically dependent cross-linking hydrogels. *Adv. Mater.* **2015**, *27*, 6283−6288.
(60) Dilla, R. A.; Motta, C. M. M.; Xu, Y.; Zander, Z. K.; Bernard, N.; Wiener, C. G.; Vogt, B. D.; Becker, M. L. Mechanically tunable, human mesenchymal stem cell viable PEG-oxime hydrogels with invariant precursor composition, concentration, and stoichiometry. *Mater. Today Chem.* **2019**, *11*, 244−252.
(61) Smith Callahan, L. A.; Childers, E. P.; Bernard, S. L.; Weiner, S. D.; Becker, M. L. Maximizing phenotype constraint and extracellular matrix production in primary human chondrocytes using arginine-

https://doi.org/10.1021/acs.macromol.1c00765
Macromolecules XXXX, XXX, XXX−XXX

glycine-aspartate concentration gradient hydrogels. *Acta Biomater.* **2013**, *9*, 7420−7428.
(62) Endres, K. J.; Xie, T.-Z.; Chakraborty, S.; Hoopingarner, C.; Wesdemiotis, C.; Wesdemiotis, C. Monitoring metallo-macromolecular assembly equilibria by ion mobility-mass spectrometry. *Macromol. Rapid Commun.* **2019**, *40*, 1800667.
(63) Fairbanks, B. D.; Schwartz, M. P.; Bowman, C. N.; Anseth, K. S. Photoinitiated polymerization of PEG-diacrylate with lithium phenyl-2,4,6-trimethylbenzoylphosphinate: Polymerization rate and cytocompatibility. *Biomaterials* **2009**, *30*, 6702−6707.
(64) https://spectrabase.com/spectrum/Kwx2NG5DoaO (accessed on July 14, 2021).
(65) https://chem.libretexts.org/Bookshelves/Physical_and_Theoretical_Chemistry_Textbook_Maps/Supplemental_Modules_(Physical_and_Theoretical_Chemistry)/Chemical_Bonding/Fundamentals_of_Chemical_Bonding/Bond_Energies (accessed on July 14, 2021).
(66) Wesdemiotis, C.; Solak, N.; Polce, M. J.; Dabney, D. E.; Chaicharoen, K.; Katzenmeyer, B. C. Fragmentation Pathways of Polymer Ions. *Mass Spectrom. Rev.* **2011**, *30*, 523−559.
(67) Snyder, S. R.; Wesdemiotis, C. Elucidation of low molecular weight polymers in vehicular engine deposits by multidimensional mass spectrometry. *Energy Fuels* **2021**, *35*, 1691−1700.
(68) O'Neill, J. M. Using atmospheric solids analysis probe mass spectrometry (ASAP-MS) for the analysis of polyester based cross-linked networks. In *Multidimensional Mass Spectrometry Studies on Amphiphilic Polymer Blends and Cross-Linked Networks*. Ph.D. Dissertation, The University of Akron, 2021, pp 75−97. https://etd.ohiolink.edu/apexprod/rws_olink/r/1501/10?p10_etd_subid=191114&clear=10 (accessed on July 14, 2021).
(69) Chen, Q.; Cui, X. F.; Zheng, W. J.; Zou, W.; Li, Y.; Yan, J.; Yang, H.; Yang, F.; Zhang, H. B. Hydrogels containing modified ammonium polyphosphate for fireproof materials. *J. Appl. Polym. Sci.* **2021**, *138*, 51007.
(70) Ma, L.; Huang, X.; Sheng, Y.; Liu, X.; Wei, G. Experimental study on thermosensitive hydrogel used to extinguish class A fire. *Polymers* **2021**, *13*, 367.

https://doi.org/10.1021/acs.macromol.1c00765
Macromolecules XXXX, XXX, XXX−XXX